8-12-2016

Deciphering Phosphorus and Aluminum Physiochemical Associations in Paleolake Sediments of Long Pond, GA

Christopher Tidwell

DECIPHERING PHOSPHORUS AND ALUMINUM PHYSICOCHEMICAL ASSOCIATIONS IN PALEOLAKE SEDIMENTS OF LONG POND, GA

by

CHRIS TIDWELL

Under the Direction of Nadine Kabengi (PhD)

ABSTRACT

This study focuses on Long Pond, a groundwater-fed sinkhole lake in Georgia, which does not exhibit any evidence of eutrophication drivers despite high concentrations of sedimentary phosphorus (P) (> 3000 mg/kg P) in the recent sediment record. Chemical analyses have shown a strong correlation (r^2>0.99) between P and aluminum (Al) throughout the core, suggesting Al plays a significant role in sequestering most of the P, and limiting its availability to phytoplankton, thereby inhibiting eutrophication. The purpose of this study is to decipher P and Al physicochemical associations in the sediments. After the samples were fractionated into amorphous and non-amorphous phases, the correlation was maintained in both phases. Evidence suggests two modes of Al-P associations : a sorption and/or co-precipitation occurring mostly in the amorphous phase and a mode whereby Al and P are being inputted to the lake bound together.

INDEX WORDS: Phosphorous, Eutrophication, Paleolimnology, Lake Sediments, Aluminum, Geochemistry

DECIPHERING PHOSPHORUS AND ALUMINUM PHYSICOCHEMICAL ASSOCIATIONS IN PALEOLAKE SEDIMENTS OF LONG POND, GA

by

CHRIS TIDWELL

A Thesis Submitted in Partial Fulfillment of the Requirements for the Degree of

Master of Science in the College of Arts and Sciences

Georgia State University

2016

DECIPHERING PHOSPHORUS AND ALUMINUM PHYSICOCHEMICAL ASSOCIATIONS IN PALEOLAKE SEDIMENTS OF LONG POND, GA

by

CHRIS TIDWELL

Committee Chair: Nadine Kabengi

Committee: Dan Deocampo

Matthew Waters

Electronic Version Approved:

Office of Graduate Studies

College of Arts and Sciences

Georgia State University

August 2016

DEDICATION

I would like to dedicate this thesis to my wife, Kirsten. Your patience, understanding, and support have been unwavering throughout this process. I truly could not have done it without you.

ACKNOWLEDGEMENTS

I would like to thank all the professors, staff, and fellow students in the Georgia State University Geosciences Department for their many contributions to my academic journey. Special thanks to Bonnie Sams, Dr. Robert Simmons, Nathan Rabideaux, and David Davis for their help and support.

I would like to thank Dr. Deocampo for serving on my thesis committee and providing amazing advice on my research. I would like to thank Dr. Waters for initiating this fascinating research question and all his many contributions and assistance to this thesis. Finally, I would like to thank my advisor, Dr. Kabengi, who has been constant in her support, assistance, and belief in my ability to produce this work.

TABLE OF CONTENTS

LIST OF TABLES

LIST OF FIGURES

1 INTRODUCTION

Eutrophication is a process whereby phytoplankton grows in abundance to the detriment of the health of aquatic ecosystems. The sudden, rapid increase of phytoplankton population causes a deficit of oxygen and light to the depths of the water. This lack of oxygen and light can then lead to massive death of plant and animal species that dwell below the surface (Read et al., 2014). Among many other factors, excess concentrations of Phosphorus (P) in the water column can be one of the leading causes of eutrophication in bodies of water (Schindler, 1977; Xu et al., 2014).

Human activity can accelerate the process of eutrophication, as anthropogenic sources of P like septic tanks, waste water treatment plants, and modern agricultural practices greatly surpass natural processes, such as natural precipitation, by which P is immobilized (Bennett et al., 2001). These anthropogenic activities increase P runoff into nearby aquatic ecosystems either in the form of transported nanoparticulate or soluble species (National Research Council, 1993). Mobilization of particulate P by erosion and runoff is the dominant form of P input into bodies of water (Sharpley et al., 1992 , Smith et al.,1992). The amount of P that will be available to the surrounding solution and hence potentially to eutrophication is a function of the soil's ability to retain and release P (Busman et al., 2002; Tiessen, 1995).

Solubility and the kinetics of P release from soil compounds are influenced by changes in pH, ionic strength, as well as the concentration of other anions and cations in the soil solution (Devau et al., 2009; Hinsinger et al., 2009). Soluble P is usually available when the soil's P-adsorbing phases, such as iron (Fe), aluminum (Al) and calcium (Ca) oxides and oxyhydroxides, are saturated and can no longer sorb additional P (Sims et al., 1998), and Al-, Fe-, and Ca-

phosphates all have different solubility properties (McDowell & Sharpley, 2003). This means that Al, Fe, and Ca content in soil greatly contribute to the amount of soluble P.

However, not all soluble P will be available to the phytoplankton of a lake (Devau et al., 2009; Kawasaki et al. 2010; Shariatmadari et al., 2006). P availability to phytoplankton, and hence the potential for eutrophication, is correlated to the form and speciation of P present in the lake. (McDowell & Sharpley, 2003). Orthophosphates ($H_2PO_4^-$ and HPO_4^{2-}) are the forms most available for assimilation by phytoplankton under pH ranges found in natural waters (Figure 1; (Petergans, 2008). However, orthophosphates can be removed by precipitation with Al^{3+}, Fe^{3+}, and Ca^{2+} (Spikatov et al, 1999) to form amorphous and crystalline metal oxides depending on time and in situ chemical conditions.

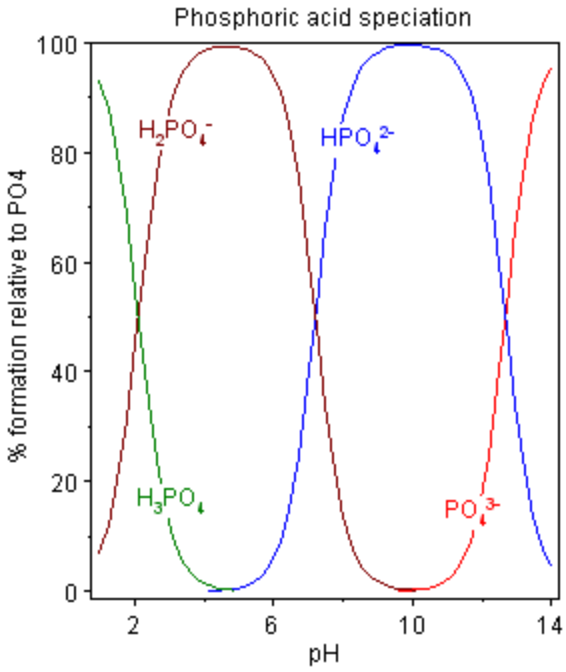

Figure 1: Phosphate speciation related to pH (Petergrans, 2008)

The presence of P in a core sample is a strong indicator of phosphorus inputs into a lake, which can be a driver of eutrophication (Kenney et al., 2002). P fractionation, speciation and how it adsorbs to oxides can yield significant information about how P has aged within a closed environment, such as a shallow lake (Jalali & Ranjbar, 2010). Adsorption and transformation of P species is key to understanding the paleoenvironment of a lake and pinpointing the sources of excess P in a lake ecosystem (Aspila et al., 1976; Van Nieuwenhuyze et al., 2014).

This study focuses on Long Pond, a groundwater-fed sinkhole lake in south Georgia, USA, which does not exhibit any evidence of eutrophication despite high concentrations of P (> 3000 mg/kg) measured in the upper parts of its sediment record. Other lakes at similar concentration have usually been eutrophied (Kenney et al, 2016; Kenney et al., 2002; Waters et al, 2005) . The range of P concentration for a body of water considered to be eutrophic can be as low as ~500 mg/kg (Hagerthey et al, 2008; L.-H. Kim et al, 2002). Evidence of abundant algae, phytoplankton, and diatoms in the lower depths of the core (500-300cm), suggests eutrophic conditions were not prominent in most of the lake's history. The absence of eutrophication still holds despite a steady increase of the P concentrations in the upper sediments of the core. Measured P concentrations ranged from around 200 mg/kg to > almost 3000 mg/kg (Earley, 2015).

Chemical analyses have shown a strong correlation (r^2>0.99) between P and Al throughout the 500-cm core, and along with the absence of eutrophication, indicates that Al plays a significant role in sequestering available P and potentially inhibiting eutrophication in the lake (Earley, 2015).

1.1 Purpose of the Study

The purpose of this study is to decipher the physicochemical associations of P and Al in the sediments of the Long Pond sediment core. If this Al-P relationship has existed throughout the history of the lake, a pertinent question to answer will be whether this signal is detrital or authigenic. Findings from this work will elucidate the relationship between the P and Al in Long Pond and help explain the lack of eutrophication. These findings will aid in understanding why some freshwater bodies with high levels of P experience eutrophication and others do not.

2 BACKGROUND

This work examines samples taken from a sediment core of Long Pond located in the Lake Park, Ga. Area. The site lies with in the Coastal Plain geological province of Georgia (Figure 2)(GeorgiaInfo, 2016), an area dominated by undeformed sedimentary formations from the Late Cretaceous to the present day Holocene epoch (Frazier, 2016). Long Pond and the other natural sinkhole lakes in this area are connected to the upper Florida Aquifer System (Hyatt & Gilbert, 2003). Long Pond consists of 3 separate sinkhole basins. It is 2.5 km^2 in area with an average depth of 4.3 m. The sediment core for this work was collected from the middle basin (Figure 3), where the maximum depth of 8 m can be found (Earley, 2015)

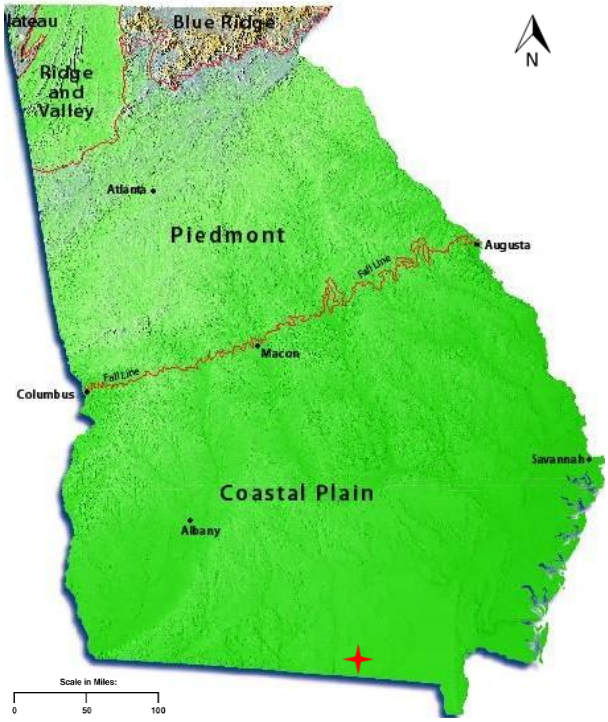

Figure 2: Map of Georgia with geologic regions. Lake Park, Ga marked with red star.

Figure 3: Inset of Long Pond in Lake Park, Ga showing 3 sinkhole basins. Coring was conducted in middle basin at the deepest part of the lake.

2.1 Characterization of Site Area

2.1.1 Geological

The site area was classified for rock type and geological formations using geological map data from the United States Geological Survey(USGS) (Huddlestun, 1997) (Figure 4). Study area specific geological maps were created using ArcGIS and USGS data. Long Pond resides in an area dominated by Neogene clay and mud with older sand (Pleistocene-Pliocene) and Mississippian sandstone nearby. Long Pond itself is located in the Pliocene Miccosukkee Formation shown in Figure 4. The lithology of this section is mostly sand with thin beds of clay. Of particular note is the nearby Statenville formation member of the Miocene Hawthorne group, located directly east of Long Pond (Figure 4, in green). The lithology of the Statenville formation contains clay, dolostone and phosphatic rock.

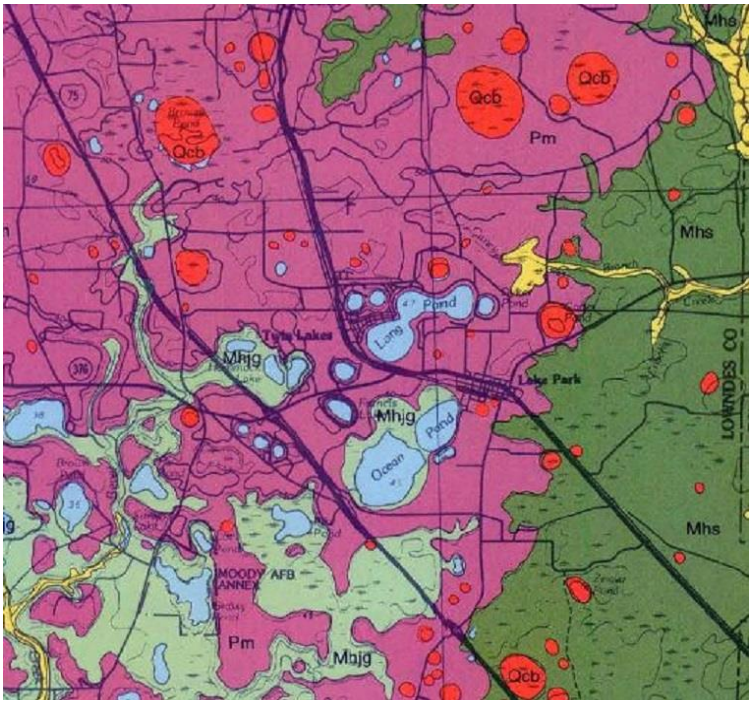

Figure 4: Geological Units of the Long Pond area. The Pliocene Miccosukkee Formation in pink and the Statenville Formation in Green (Huddlestun, 1997).

2.1.2 Hydrological Maps/Watershed

Small, site area specific watersheds were created using ArcGIS and Digital Elevation Map (DEM) data from the USGS (Figure 5). Small value thresholds were selected for accumulation and stream link rasters in order to provide small watersheds isolated to Long Pond and the surrounding lakes in the area. This was done to identify possible surface water source inputs, particularly P and Al from anthropogenic sources.

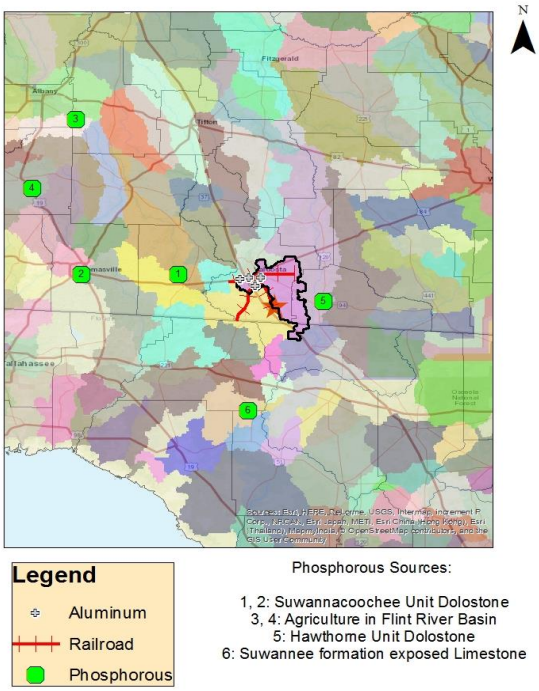

Figure 5: Watershed Map of Long Pond area. Possible sources of phosphorous and aluminum are highlighted.

USGS groundwater contour data on the Floridian aquifer was added to a map of the site area to guide in the identification of possible groundwater sources of P and Al (Figure 6).

Though there are other phosphate containing formations nearby, the Statenville formation is the only formation within a close enough proximity to provide P input to Long Pond.

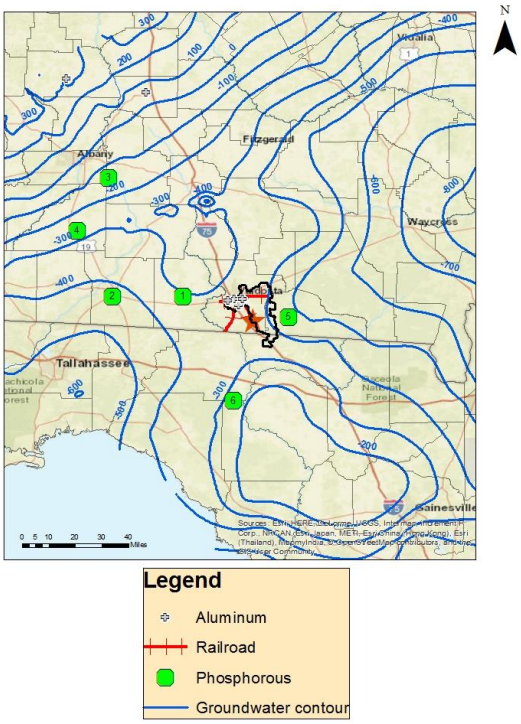

Figure 6: Groundwater contour map of Long Pond area with possible sources of aluminum and phosphorus highlighted.

2.1.3 Historical Divisions of Long Pond

Earley's initial work included the dating of the sediment core. The core was dated by excess ^{210}Pb and ^{14}C dating analysis (Schelske et al, 1994; Appleby and Oldfield, 1983). Earley used K-means cluster analysis of nutrients, organic matter content (Loss on Ignition), phytoplankton primary producer abundance and Carbon to Nitrogen ratios to differentiate 3 different zones of Long Ponds limnological history (Figure 7). Primary producer abundance as inferred from measurements of photosynthetic pigments was plotted against depth to show relative highest and lowest points of phytoplankton abundance. Earley's work shows little evidence of eutrophication in Long Pond even at its highest point of P concentration at the top 100 cm of the core.

Zone 1 covers 500 cm to ~ 300 cm of the core, and represents a time when the location was a shallow wetland dominated by highly organic, peaty sediments. Zone 1

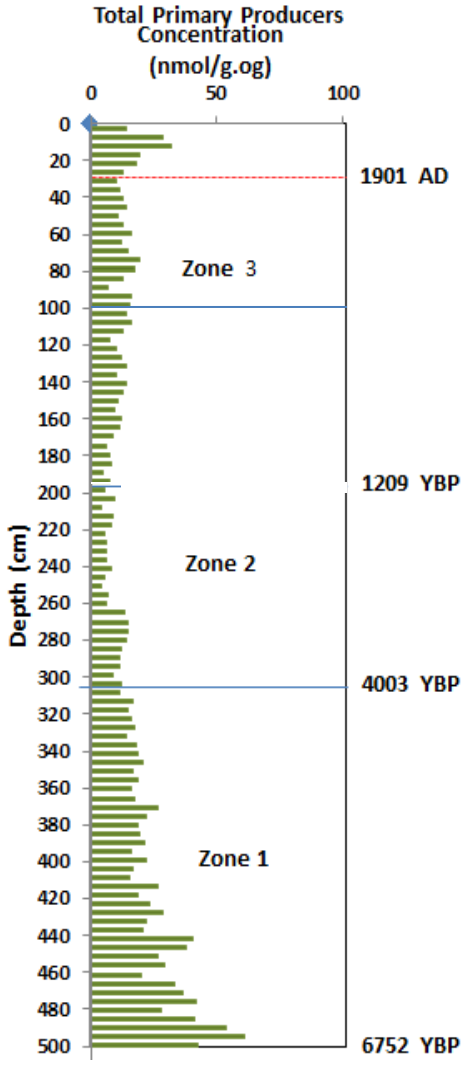

Figure 7: Concentration of phytoplankton primary producers. v. depth. Historical boundaries marked with approximate age. Chart taken from Earley, 2015 and used with permission.

also shows the highest amount of phytoplankton evidence.

Zone 2, ranging from ~300 cm to ~96 cm, shows a change from wetland to a transitional lacustrine environment. During this period, the lake would develop increased connectivity to the surrounding watershed resulting in increased inputs of nutrients. This corresponds to a possible increase in precipitation and sea level rise, or a changed in the hydrology in this area at the end of Zone 1's time period (Colquhoun et al., 1995).

Zone 3, marked as above 96 cm, indicates the period of the modern lacustrine environment of Long Pond. While still in Zone 3, the ~30 cm mark is notable as an indication of increased anthropogenic inputs into the lake system. This depth is estimated to represent ~ 1900 AD, soon after the building of a nearby railroad, and during a time of general increase in more industrialized human activity.

3 METHODS

3.1 Coring

This project was conducted in conjunction and as an extension of earlier work by Sean Earley, M.S. from Valdosta State University, Biology Department, under the direction of Dr. Matt Waters. In December 2012, a 500-cm piston core was collected from Basin #2 of Long Pond, in Lake Park, GA (Earley, 2015). This site was chosen based on soft sediment survey of the lake, deeming it the best depositional area (Earley, 2015).

As part of this work, an additional coring of the mud/water interface was done in January 2016 in the same basin to collect more sediment for additional analysis. In addition, two 10-cm soil samples were taken 2 meters inland from shore locations close to Lake Pond for comparison to lake sediments.

All cored samples were freeze dried and kept in plastic bags until further analysis.

3.1.1 Sample Selection

Freeze dried samples were chosen from depths of 4-8, 16-20, 32-36, 44-48, 150-155, 200-205, and 475-480 cm for analysis (Table 1). These depths represent significant dating points and are chosen for their proximity to paleolimnological transitions in the lake as discussed previously in section 2.1.3.

Table 1: Sample Selection Criteria

Depth (cm)	Zone/Boundary	Represents:
4	**Top of Core**	**Most recent, largest anthropogenic inputs**
32	**1900 AD boundary**	**Beginning of modern anthropogenic influence**
44	**Zone 3**	**Before modern anthropogenic influence**
200	**Zone 2/Zone 3 border**	**Transition to present lacustrine system**
475	**Zone 3**	**Early period of lake's history; Wetland**

3.2 Mineralogical Analysis

Samples were examined for minerals using X-ray diffraction (XRD) with a Philips model 12045 X-ray diffractometer, using Cu Kα radiation at 45kV and 40mA and filtered by a .020 Nickel Beta-filter with a fixed, programmable 1/2° anti-scatter slit and a programmable 1/4° divergence slit. Three types of samples treatments were analyzed, as described below.

3.2.1 Whole sample, no treatment

Ground, freeze dried, untreated samples were examined by XRD to determine presence of crystalline minerals. Samples were mounted on zero background mount and scanned from 5 to 65°2θ in continuous scan mode.

3.2.2 Clay fraction, no treatment

Samples were washed, sonified, and centrifuged to separate the clay fraction for further XRD analysis. Carbonates were removed by shaking samples in 0.5 M HCl for 1 hour, then centrifuged and rinsed in deionized water (Ulery and Drees, 2008). The intent of the carbonate removal procedure was to reduce noise in the XRD signal observed on whole samples. Wet samples were mounted on glass slides, air-dried and scanned from 5 to 65°2θ in continuous scan mode.

3.2.3 Carbonate and Ammonium Oxalate treatment

Additional oven dried samples from all depths listed in Table 1 were ground, sieved with a number 120 sieve (125 μm), and subjected to carbonate removal by 0.5 M HCl as described above. These samples were subjected to ammonium oxalate dissolution in the dark procedure to remove amorphous metal oxides phases (Ulery and Drees, 2008). Samples were shaken in 0.2 M ammonium oxalate solution for 4 hours without exposure to UV light. A detailed description of this procedure in included in section 3.4.2. Following the dissolution of amorphous phases, remaining solid samples were washed and air-dried, then examined by XRD on a continuous scan mode from 5 to 65°2θ in order to classify crystalline mineralogy.

3.3 Electron Microscopy Analysis

Ground, freeze dried samples from the 4-8 cm, 44-48 cm, 150-155cm, 200-205 cm, and 475-480 cm depths were chosen for analysis by electron microscopy to study the general morphology of the samples and possibly identify any P-containing mineral and/or biological phase that might be present in the sediments of significant depths. A LEO 1450vp scanning electron microscope (SEM) was used. Samples were mounted on aluminum stubs and sputter-coated with carbon paint to prevent electron build up on surfaces. Information on representative elemental composition from selected areas on the samples was collected using energy dispersive X-ray spectroscopy (EDS; Rontec X-Flash detector).

3.4 Chemical Analysis

3.4.1 Initial Analysis by Earley

Earley measured the concentrations of organic matter by a loss on ignition (LOI) method at 550°C. For chemical elemental compositions, samples were digested using standard EPA 3050 method and analyzed by Inductively Coupled Plasma- Atomic Emission Spectrometry (ICP-AES) using an ARL 3560 ICP analyzer. Carbon/Nitrogen ratios were determined by a Costech ECS 4010 Nitrogen/Carbon analyzer after acidification by HCl vapor to remove inorganic carbon. Photosynthetic pigments were measured using High Performance Liquid Chromatography (HPLC) methods (Leavitt and Hodgson, 2001; Waters et al, 2009) to provide measurements of primary producer abundance during the lake's history.

3.4.2 Amorphous Phase Dissolution by Ammonium Oxalate

Core sediments from all depths in Table 1 were chosen for quantification of the amorphous phases. Six oven-dried samples from each selected core range were subjected to

differential dissolution by shaking in 0.2 M ammonium oxalate solution at pH 3, for a minimum of 4 hours (Ulery et al., 2008). Samples were allowed to settle then centrifuged at 8500 RPM for approximately 45 minutes until a clear supernatant was obtained. This dissolution was carried out without exposure to UV light at all stages, in order to preferentially dissolve amorphous Si, Fe, and Al, and preserve crystalline species of Si, Fe, and Al in the solid phase. All samples were kept in opaque containers and handled in labs with limited light exposure. Extra precautions were taken during handling and transport of samples to prevent exposure to all light. No glass lab wear was used in the dissolution process to prevent any addition of Si from lab wear. The clear supernatant was then vacuum filtered using a 0.35μm non-glass fiber filter. Samples were carefully weighed before the procedure and again at the end after being washed and oven-dried in order to quantify the weight-loss attributed to the dissolution of the amorphous phases. This step is also a way to check the effectiveness of the ammonium oxalate dissolution procedure.

3.4.3 Statistical analysis/ matrix of correlations of nutrient concentrations

Using VassarStats for statistical computation (http://vassarstats.net/matrix2.html), a matrix of correlations for P, Al, Fe, Si and Organic Matter (by Loss on Ignition) values was created to check for potential correlations in each core sample depth using the concentrations values measured by Earley. This matrix built upon element concentration values obtained by Earley to provide an elemental profile related to depths of the core, and by extension its history.

Elemental concentration values obtained from the amorphous and residual non-amorphous fractions were similarly used to make a comparative matrix of correlations. Results of P v. Al, P vs. Fe, and concentrations of P, Al, and Fe against depths of the core were graphed and compared to the results from Earley.

3.5 Chemical Analysis of Amorphous and Residual Non-Amorphous Phases

3.5.1 Amorphous phase analysis

After ammonium oxalate treatment, the supernatant containing the dissolved amorphous phase from the six samples were separated into 3 10-ml aliquots and Fe, Al, and P concentrations measured by ICP-AES (ARL 3560 ICP analyzer).

3.5.2 Residual Non-amorphous phase analysis

The remaining solid phase from the above ammonium oxalate dissolutions of each sample was further divided into 3 individual samples of approximately 150mg each. These samples were digested by EPA method 3050A, and Fe, Al, and P concentrations determined by ICP-AES.

3.5.3 Whole sample analysis

An additional testing of oven-dried, carbonate removal treated samples at the same depths was conducted. Each depth sample was oven-dried, sieved (#120) and separated into 3 replicates. These samples were digested identically to the non-amorphous phase samples in the previous section and analyzed by ICP-AES to compare against results of the amorphous and non-amorphous dissolution analysis.

4 RESULTS AND DISCUSSION

4.1 XRD

Mineralogical analysis of the ground, freeze-dried, untreated samples by XRD revealed the predominant crystalline species to be kaolinite [$Al_2Si_2O_5(OH)_4$] and quartz (SiO_2) (Figure 8). There were no characteristic peaks related to an aluminophosphate minerals detected. However, the XRD signal showed a high noise-to- signal ratio, potentially masking these peaks.

Samples were then treated for carbonate removal and reduced to the clay fraction by selective centrifugation in an effort to provide a cleaner XRD analysis with less noise. Kaolinite

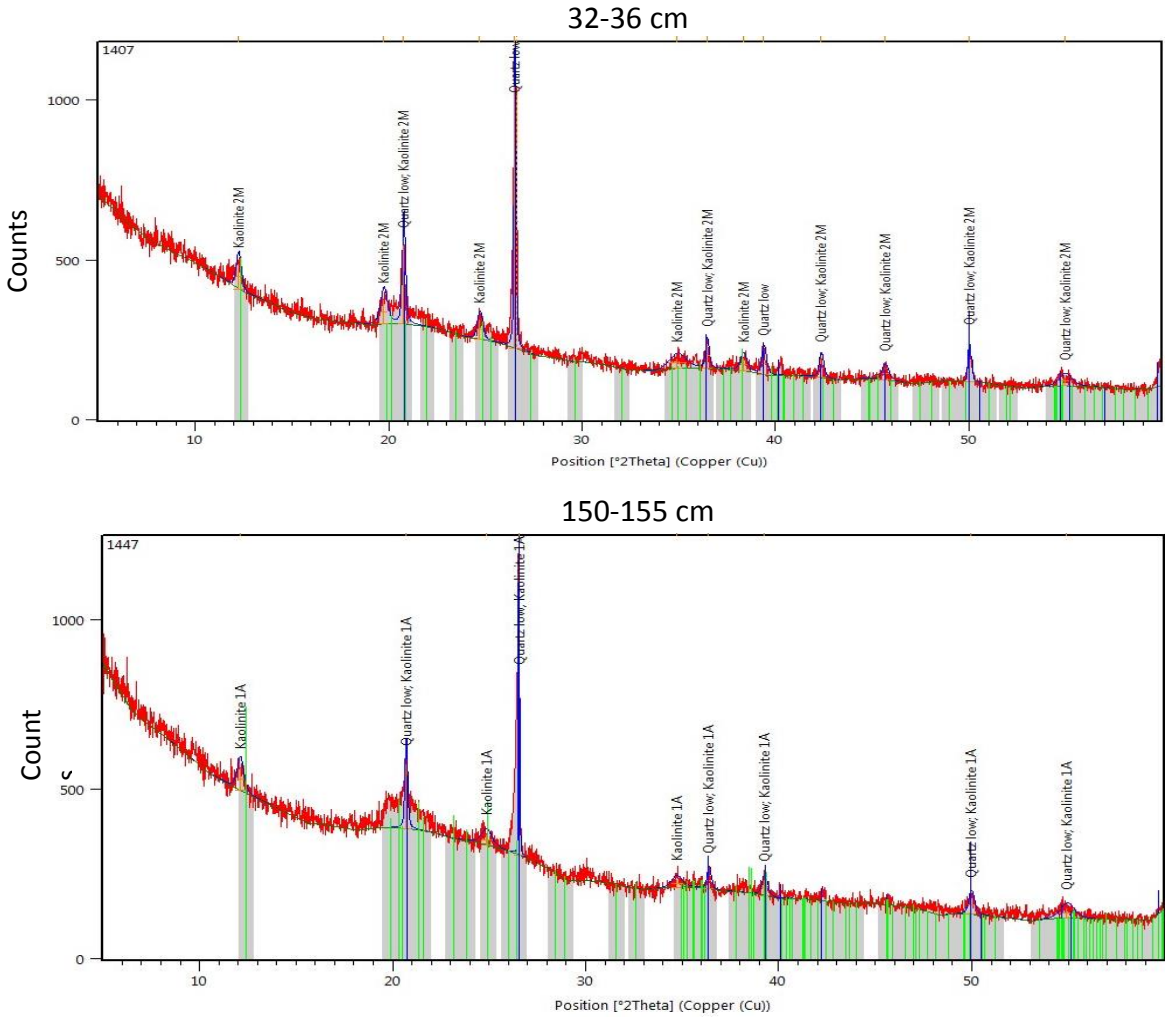

Figure 8: X-ray diffraction difractograms of whole, untreated sample showing Kaolinite and Quartz peaks

and quartz were again found to be the predominant crystalline minerals present, and no aluminophosphate mineral peaks were observed.

Following the dissolution of the amorphous phase by the ammonium oxalate procedure, the residual solid, non-amorphous phase was analyzed by XRD to determine whether the removal of amorphous phases will reveal any aluminophosphate crystalline minerals. The XRD results of these samples contained the least amount of noise, providing a clearer picture of the non-amorphous mineralogy. Again kaolinite and quartz dominated the crystalline species, and no aluminophosphate mineral peaks were found (figure 9).

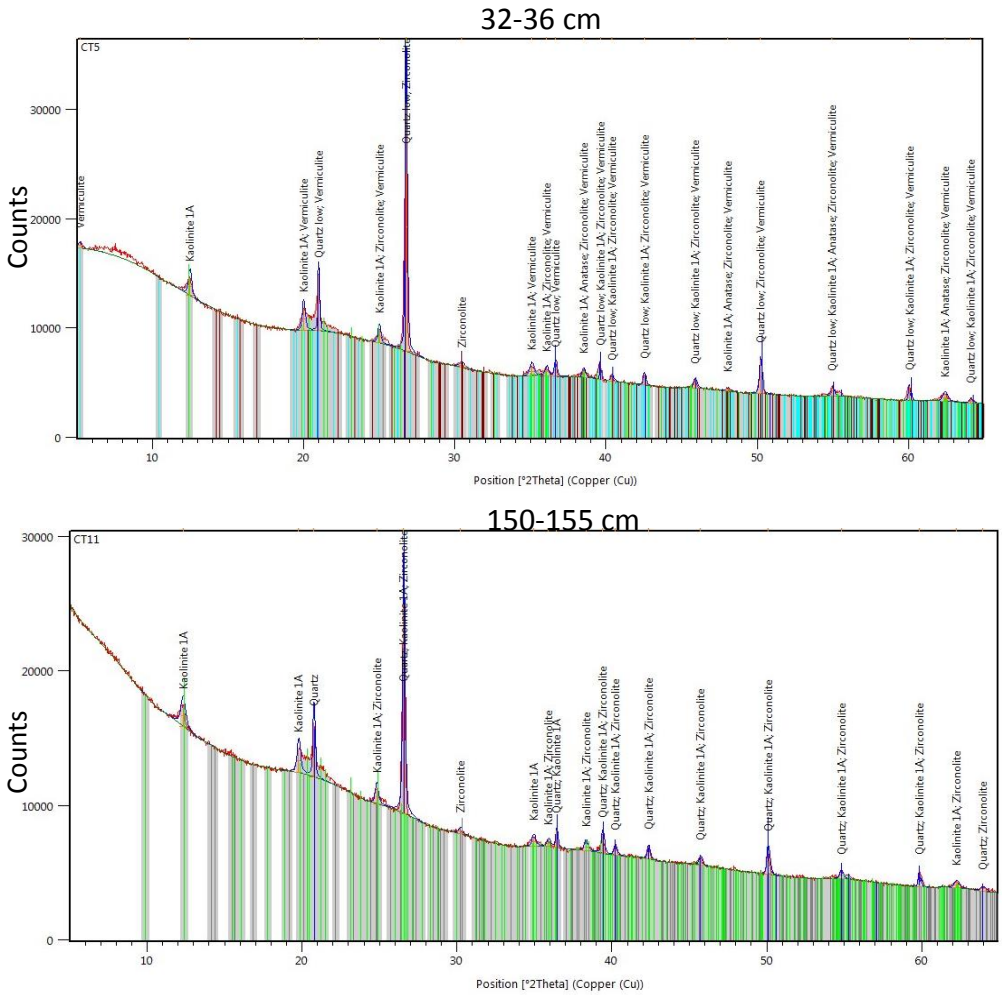

Figure 9: X-ray diffraction diffractogram of non-amorphous phase samples (as treated by Ammonium Oxalate Dissolution in the dark

XRD analysis of all samples yielded similar results, with no aluminophosphate minerals observed. Given the high concentration of P and Al, up to 3855 and 32845 mg/kg respectively, and the measured pH of the waters ranging from ~5.5 to ~7, crystalline aluminophosphate phases expected would be variscite ($AlPO_4 \cdot 2H_2O$) and wavellite [$Al_3(PO_4)_2(OH,F)_3 \cdot 5H_2O$] (Buanuam et al., 2006; Temporetti, et al., 2013). Due to the high amount of organic matter and amorphous material, the presence of these minerals may be below detection limits of XRD, which is ~1 to 2% weight of the sample in mixed samples (Dutrow & Clark, 2008; Moore, 1997; Ulery et al., 2008) . The detection can also be affected by particle size (Kim et al., 1996). Ideal particle size for detecting crystalline phases in XRD is 10-50 μm (Pecharsky & Zavalij, 2008). It is possible that these samples contain small crystallites of aluminophosphate minerals that are not large enough to be detected.

4.2 SEM

Scanning electron microscopy analysis of the samples showed mostly organic matter and silica (Figure 10), as also indicated by the EDS analysis.

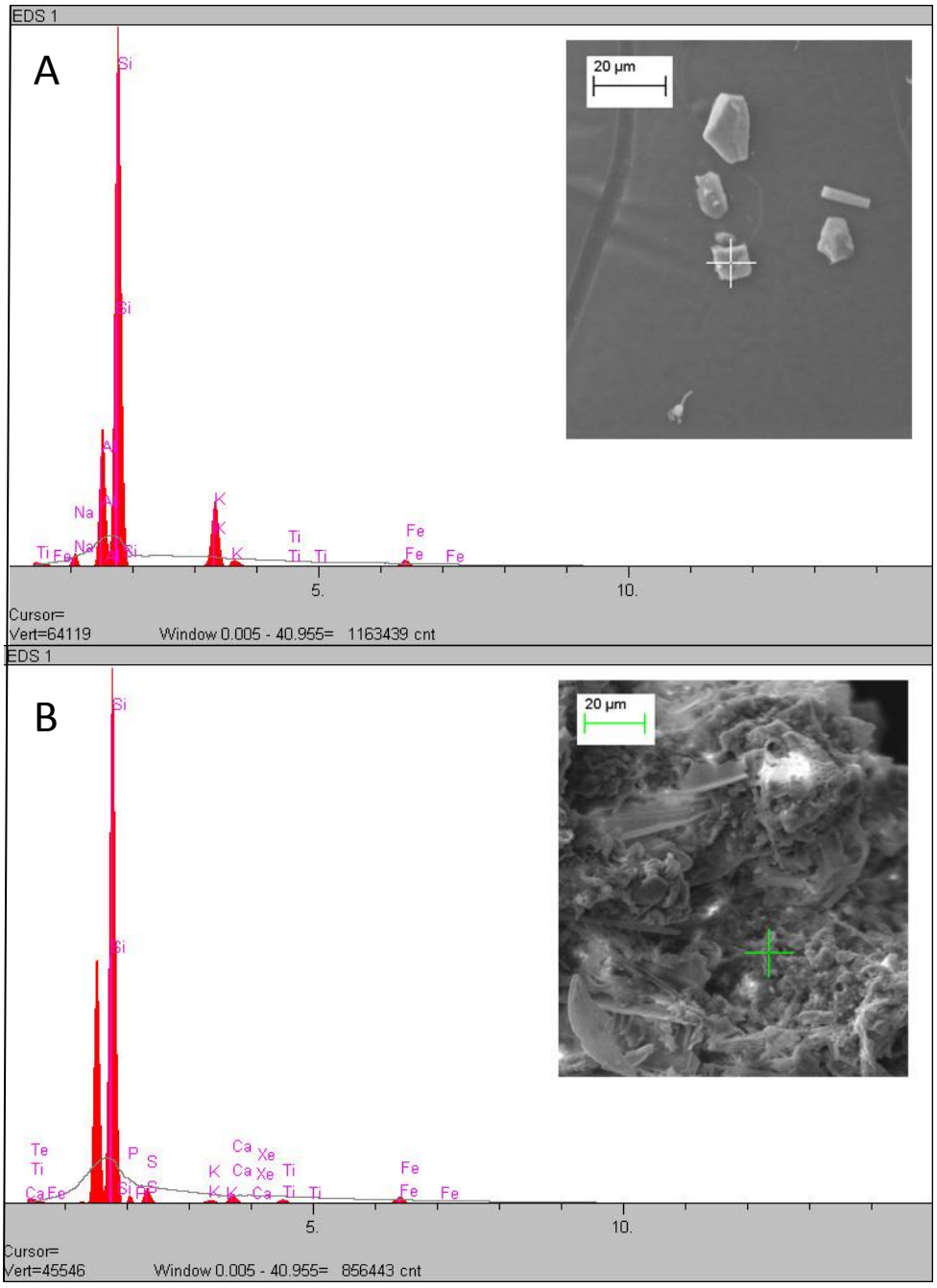

Figure 10: Scanning electron micrographs and corresponding energy dispersive X-ray spectroscopy data of top 4-8 cm. Panel A shows grain with high silica content. B shows organic matter with high silica content.

Some aluminosilicate minerals were seen as well. Based on the previous XRD results and their morphological similarity to published specimens from the clay mineral society database (figure 11), these were identified as kaolinite and gibbsite (Bohor & Hughes, 1970; Welton, 2003).

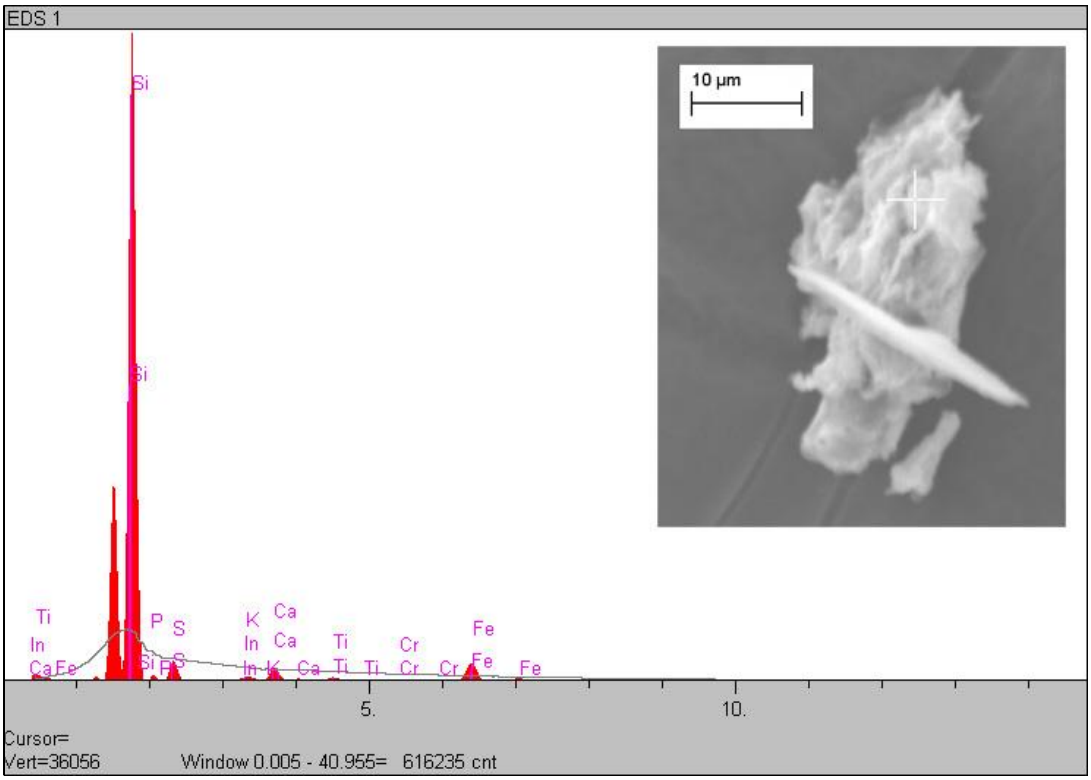

Figure 11: Scanning electron micrograph and energy dispersive X-ray spectroscopy data showing an aluminosilicate specimen obtained from a sample taken at 4-8 cm depth.

From all samples viewed and spots analyzed by EDS, there was one instance where the presence of both P and Al was detected concurrently in the same spot from a round grain found in a sample taken from the top 4-8cm of the core (Figure 12). Given that SEM is mainly a surface technique, it is unclear at the moment whether the round grain is an aluminophosphate phase in its entirety or whether the Al-P phase is a coating of the mineral. The presence of the Si (Kα peak at around 1.7-1.8 keV) would suggest the concurrent presence of an aluminosilicate. It is also noteworthy to mention the presence of a calcium peak (Kα at 3.690 keV) that appears to be more prominent.

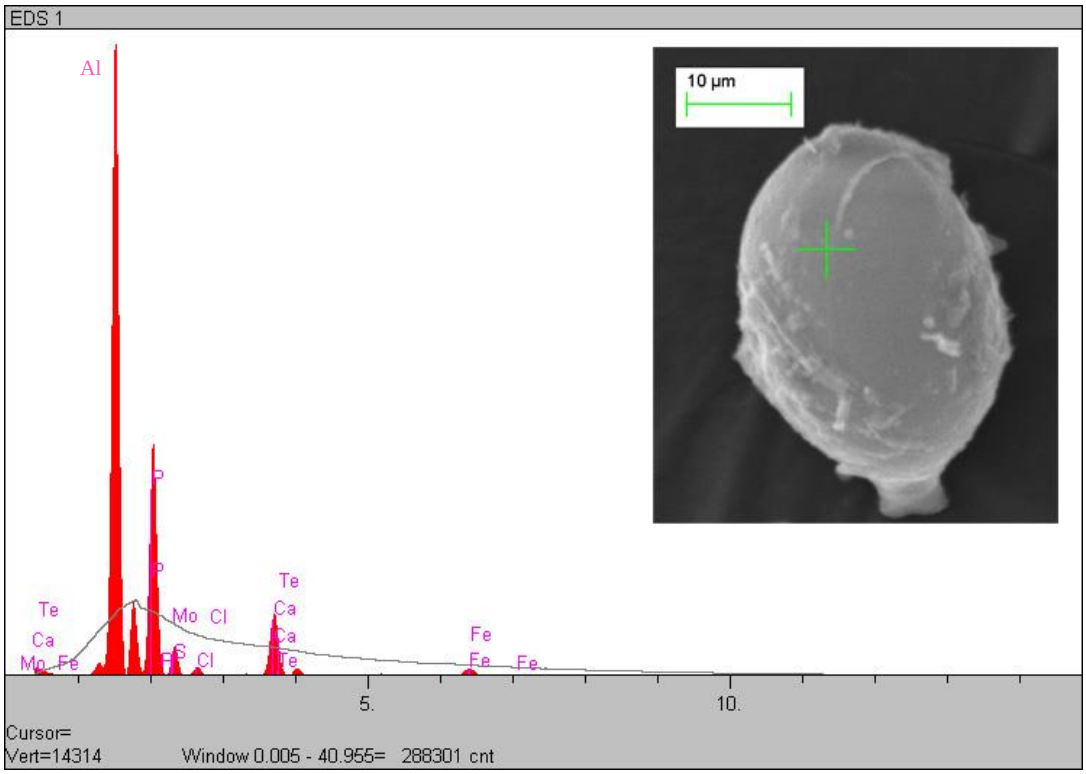

Figure 12: Scanning electron micrograph and energy dispersive X-ray spectroscopy showing a specimen containing Al and P obtained from a sample taken at 4-8 cm depth

Samples from the bottom of the core (425-430cm; Figure 13) showed a high density of silica bearing spicules, seemingly from a freshwater invertebrate species.

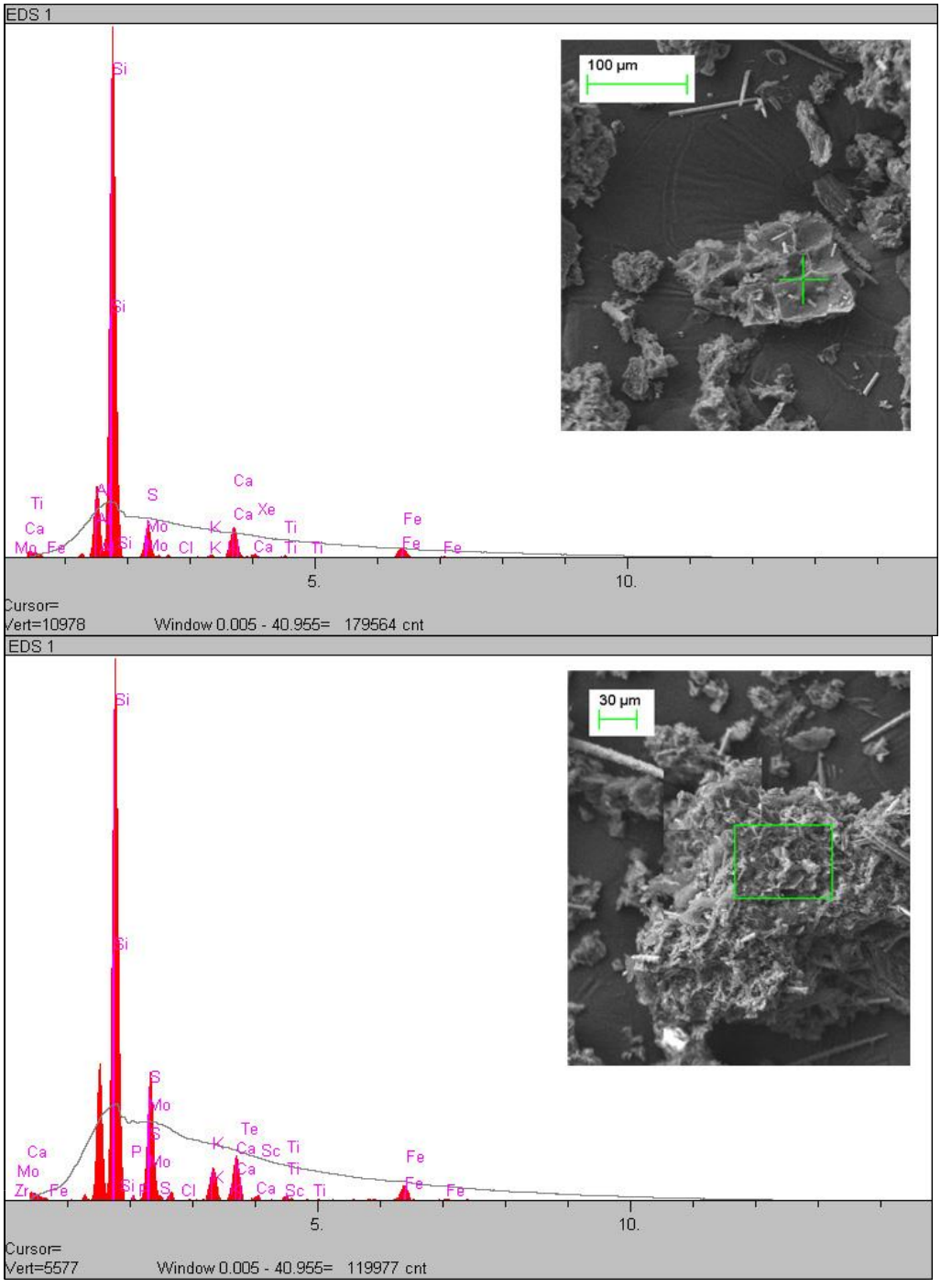

Figure 13: Scanning electron micrograph and energy dispersive X-ray spectroscopy data showing organic matter and silica-bearing spicules from 425-430 cm depth

4.3 Weight Analysis of Amorphous Dissolution by AOD

Table 2 displays the mean weight of samples from each depth, before and after the dissolution of the amorphous phases was conducted. Overall samples exhibited between 11.10 % and 25.04 % weight loss with samples from the bottom of the core losing more mass than samples from the top. The mass loss is attributed to the dissolution of amorphous phases of Al, Fe and Si oxides. This result is to be expected, as samples from the bottom of core belonged to zones 1 and 2, when the lake was identified as being a wetland and transitional lacustrine environment and therefore could have lost some of their high organic matter and potentially some of the more amorphous silica bound to the much abundant invertebrate species. Nevertheless, these values are a bit surprising to us because it is the upper parts of the core that had the highest concentrations of Al and P, and since no crystalline mineral phase was detected by XRD, we were expecting the samples to contain a higher percentage of amorphous phases.

Table 2: Mass loss due to ammonium oxalate dissolution

Depth	Initial Weight (mg)	Final Weight (mg)	% loss[±]
4	252.53 (± 2.3)[*]	218.87 (± 1.3)[*]	13.33
32	252.47 (± 1.6)[*]	222.43 (± 1.1)[*]	11.90
44	251.6 (± 1.0)[*]	223.67 (± 2.1)[*]	11.10
150	251.97 (± 0.6)[*]	210.07 (± 1.3)[*]	16.63
200	251.33 (± 0.9)[*]	188.4 (± 3.6)[*]	25.04
457	251.67 (± 0.2)[*]	194.3 (± 6.4)[*]	22.80

[*] Number in parenthesis are the mean standard deviations
[±] Values in this column are obtained by the following formula (Initial weight – final weight)/initial weight

A possible reason why the recovery of the amorphous phases may not be totally representative is the seeming ineffectiveness of the AOD dissolution method to account for the

high organic matter content of the samples which ranged from 30% to 79% OM by LOI. In fact, an attempt at mass balancing P, Al and Fe concentration between total, amorphous and residual or non-amorphous, returned overall low recoveries: between 71 % and 85 % for P, 51% and 68% for Al and 61% and 87% for Fe (appendix 1). The potential impact of OM on the fractionation between amorphous and non-amorphous phases can be further supported by the high negative correlation obtained between the concentrations of P and Al with the OM % by LOI (further discussed below). It is also noteworthy to mention that no correlation has been found between Fe and OM% and that overall the mass balance recoveries for Fe were overall better.

With the understanding that the absolute fractionation between amorphous and non-amorphous phases may not be totally adequate, we focus our analysis on comparative correlations between P and Al and P and Fe concentrations and their distributions along the core depths in both these fractions.

4.4 Chemical Analysis

4.4.1 Correlations

Elemental concentration data from Earley's work was plotted in a matrix of correlations to find possible relationships between P and other elements. Strong correlations (negative and positive) are highlighted in yellow (Table 3). Starting with data from Earley's experiments, a strong correlation can be seen between Al and P concentrations throughout all depths of the core. Other statistically strong correlations were found between P and Potassium (K), P and Magnesium (Mg), Al and K, Al and Mg, and Fe and Zinc (Zn). There is also a strong negative correlation of P, Al, K, and Mg with organic matter, measured by Loss on Ignition (LOI)(Table 3).

Table 3: Matrix of correlations using initial data from Earley created with Vassarstats statistical tools.

r	P	Al	Fe	Zn	Na	K	Mg	Ca	S	LOI (%)
P	1	**0.996**	0.612	0.707	-0.023	**0.97**	**0.922**	-0.01	-0.722	**-0.966**
Al	0.996	1	0.61	0.712	-0.036	**0.975**	**0.928**	-0.013	-0.721	**-0.969**
Fe	0.612	0.61	1	**0.918**	0.325	0.628	0.429	0.442	0.045	-0.511
Zn	0.707	0.712	0.918	1	0.285	0.721	0.567	0.508	-0.158	-0.575
Na	-0.023	-0.036	0.325	0.285	1	0.078	-0.17	0.289	0.155	0.116
K	0.97	0.975	0.628	0.721	0.078	1	0.853	-0.019	-0.71	**-0.948**
Mg	0.922	0.928	0.429	0.567	-0.17	0.853	1	0.003	-0.736	**-0.911**
Ca	-0.01	-0.013	0.442	0.508	0.289	-0.019	0.003	1	0.384	0.203
S	-0.722	-0.721	0.045	-0.158	0.155	-0.71	-0.736	0.384	1	0.756
LOI%	-0.966	-0.969	-0.511	-0.575	0.116	-0.948	-0.911	0.203	0.756	1

VassarStats: Correlation Matrix Number of Variables = 10 Observations per variable = 105

Of the elements that are strongly coordinated with P, Al and Fe have the highest concentrations in the core, up to 28,700 mg/kg for Al and 9,074 mg/kg for Fe. In addition, Al, Fe and Ca are the elements considered most responsible for controlling solubility of P (Frossard et. al, 2014; McDowell & Sharpley, 2003). Given the low correlation of Ca and P and the relatively low concentrations of Ca (3931 mg/kg at maximum), our subsequent analysis focuses on the correlation of P with both Al and Fe.

Al and P concentrations from 4 sets of data were plotted to show correlations. These 4 plots are shown below in Figure 14. First, initial Al and P concentrations from data from Earley were

chosen from 4 cm, 32 cm, 44 cm, 150 cm, 200 cm, and 475 cm and plotted to test correlation (Figure 14– panel A). These depths were chosen to represent the historical zones of the lake as shown in Table 1. Using the same depths, the Al and P concentrations from the untreated samples before amorphous dissolution by AOD are shown in Figure 14 – panel B. This represents the total Al and P concentrations in both amorphous and non-amorphous forms. Concentrations from the liquid phase after amorphous dissolution (Figure 14 – panel C) represent the Al and P measured concentrations in the amorphous phases. The concentrations in solid samples remaining after amorphous dissolution by AOD are plotted in (Figure 14 – panel D) and represent the non-amorphous phase of these elements.

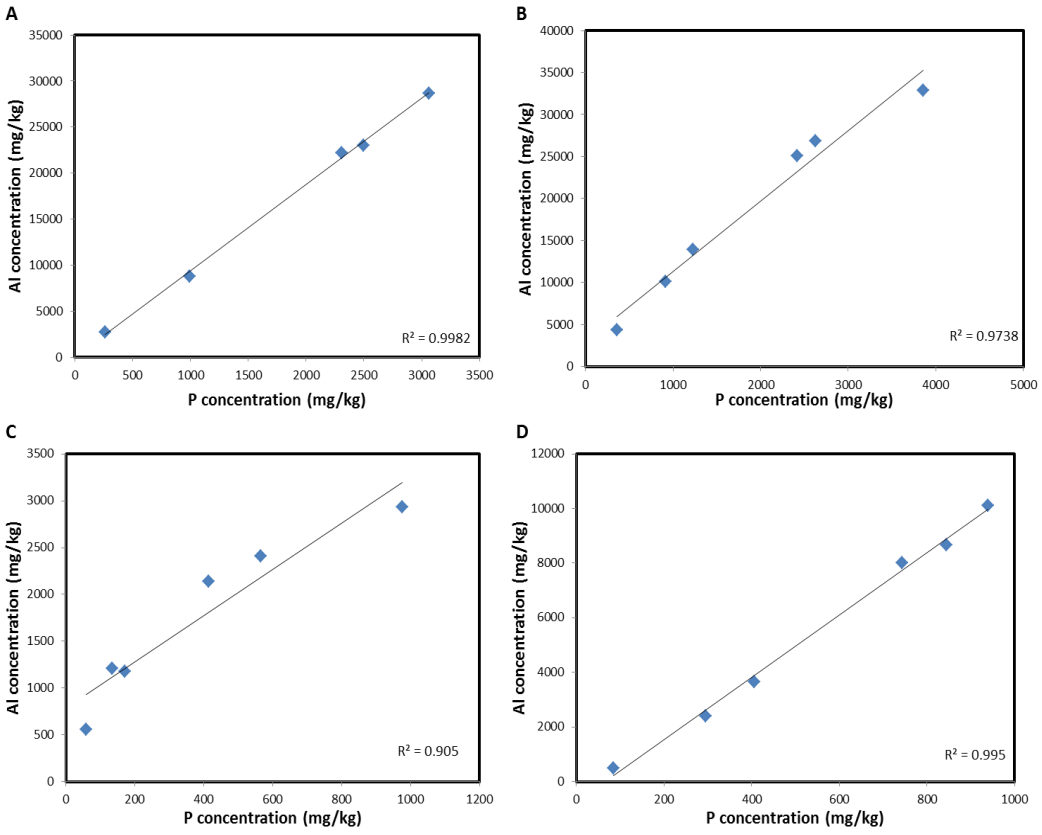

Figure 14: Al concentration v. P concentration in (A) Original samples from Earley, (B) Whole, untreated samples, (C) amorphous fractions and (D) solid samples after Ammonium Oxalate in the dark amorphous dissolution.

Correlation between non-amorphous phase Al v. P concentrations shows a slightly higher R^2 score (0.9955) than those obtained between the total Al and P concentrations in both Earley's and this study (R^2=0.9929/ 0.9738 respectively) and between the concentrations of Al and P in the amorphous phase (R^2 score 0.905).

The correlation of Fe to P concentrations were examined using the same depths and samples types used to study the Al and P concentrations correlation plots, as described above and plotted to test correlation. In Figure 15, panel A represents concentrations from Earley's original data. Panel B represents total concentrations in samples before amorphous dissolution by AOD from this study. The concentrations displayed in panel C are from the residual solid sample (non-amorphous) after AOD dissolution, and data in panel D are the concentrations of the amorphous phases recovered in the liquid supernatant.

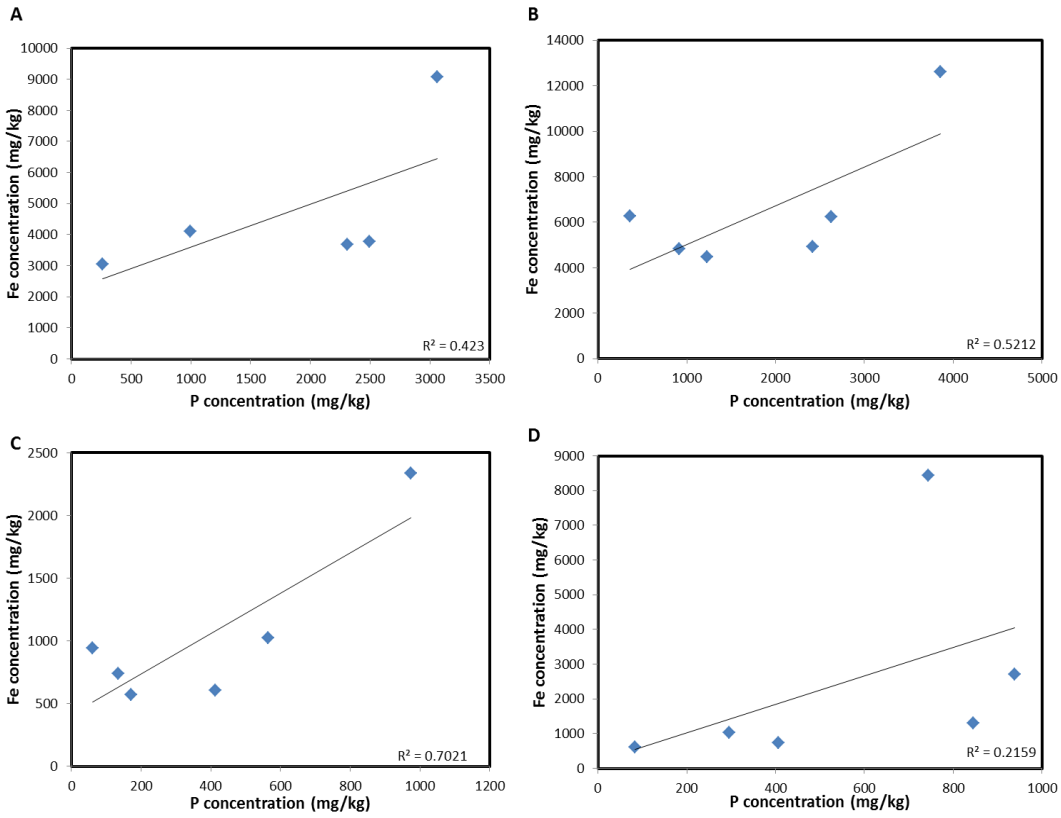

Figure 15: Fe concentration v. P concentration in (A) Original samples from Earley, (B) Whole, untreated samples, (C) amorphous fractions and (D) solid samples after Ammonium Oxalate in the dark amorphous dissolution.

In the initial analysis, Fe and P were marginally correlated (R^2=0.612). When subjected to amorphous dissolution by ammonium oxalate, the correlation between amorphous Fe and P rises to an R^2 score of 0.7021, while the non-amorphous falls to R^2=0.1259. This suggests that any correlation between the P and Fe occurs predominantly in the amorphous phase.

Correlations between the Fe and Al to P concentrations in Earley's work were similar to the correlations found in this study. The chemical analysis conducted in this study also showed that the strong relationship between Al and P holds when samples were subjected to amorphous dissolution by ammonium oxalate procedure. This suggests that Al and P could be occurring simultaneously and may be bound in both amorphous and non-amorphous phases. This persisting

correlation throughout all phases and depths also suggests that aluminophosphate species in the core would be detrital in nature.

4.4.2 Depth Profiles

Earley's elemental depth profiles show a general trend of increasing concentrations of all elements in the top 30 cm. This is consistent with heavy increase of anthropogenic inputs in the most recent history of the lake. After 30 cm, element concentrations decrease steadily down core. The organic matter content obtained by LOI shows the opposite trend with the largest amount found at the bottom of the core and decreasing as the core nears the surface. This trend reflects the paleolimnology described by Earley, as the bottom of the core represents a wetlands environment that would contain more organic matter.

Concentrations of P, Al, and Fe from Earley plotted against depth of the core were compared to concentrations of P, Al, and Fe v. depth data from samples tested before and after amorphous dissolution, and shown in the figures below.

Figure 16 shows the depth profiles of total P concentrations obtained by Earley's study in panel A), and from this study in panel B. The depth profile of P concentrations in the residual non-amorphous solids is displayed in panel C while that of the P concentration in amorphous phases is in panel D.

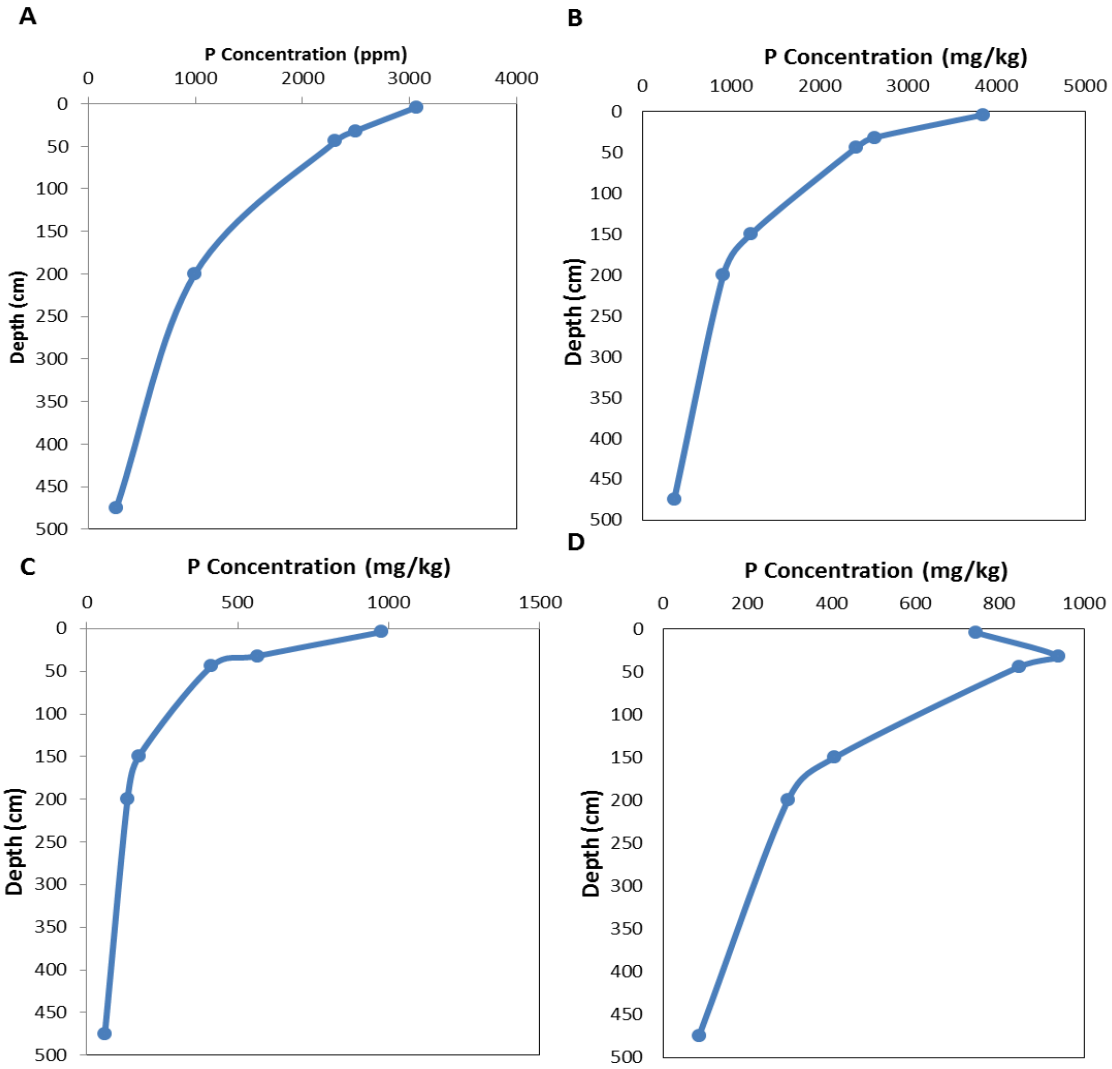

Figure 16: P concentration depth profiles (A) Original samples from Earley, (B) Whole, untreated samples, (C) amorphous fractions and (D) solid samples after Ammonium Oxalate in the dark amorphous dissolution

Figure 17 shows the depth profiles of Al concentrations obtained in A) Earley's study (panel A) and in this work (panel B). Panels C and D display the depth profiles of Al concentration in the residual solid samples (non-amorphous) retained after AOD, and liquid samples (amorphous) collected after AOD treatment respectively.

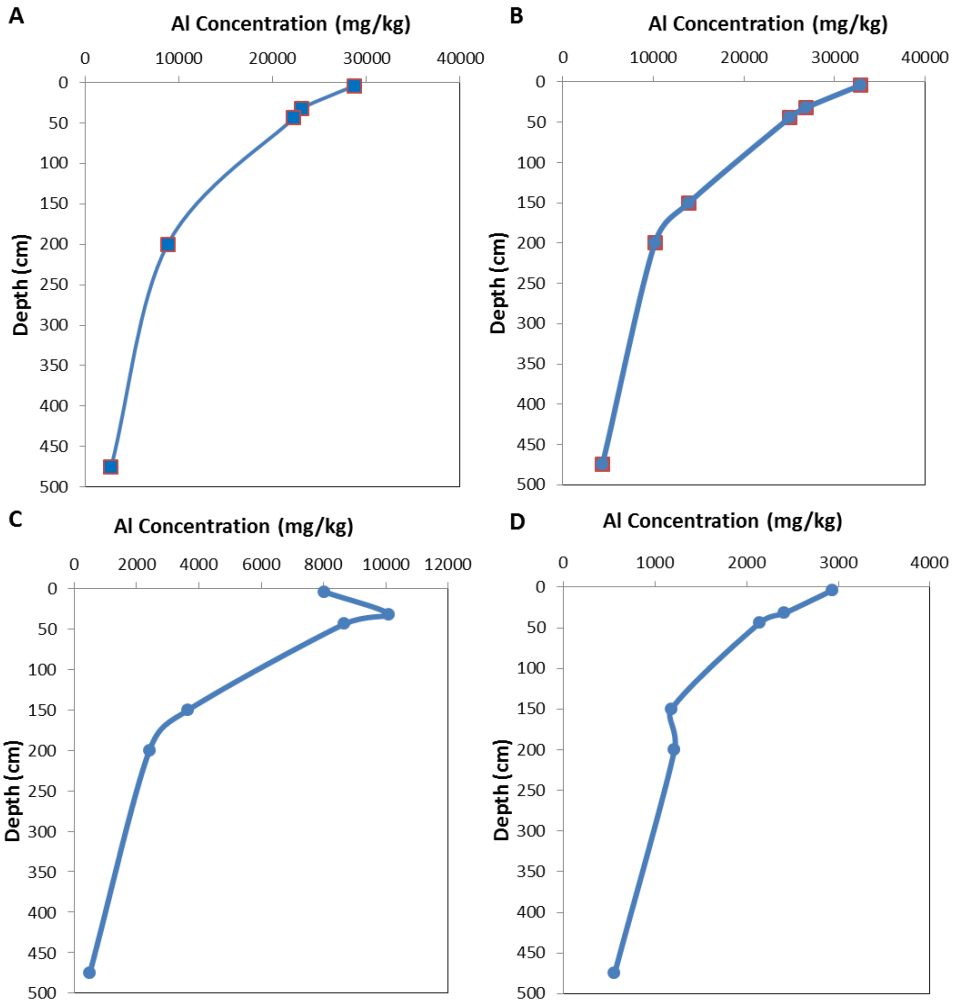

Figure 17: Al concentration depth profiles (A) Original samples from Earley, (B) Whole, untreated samples, (C) amorphous fractions and (D) solid samples after Ammonium Oxalate in the dark amorphous dissolution.

Figure 18 shows depth profiles of the Fe concentrations obtained in Earley's study (Panel A), this study (Panel B), in residual solid samples (non-amorphous) retained after AOD (Panel C), and liquid samples (amorphous) collected after AOD treatment (Panel D).

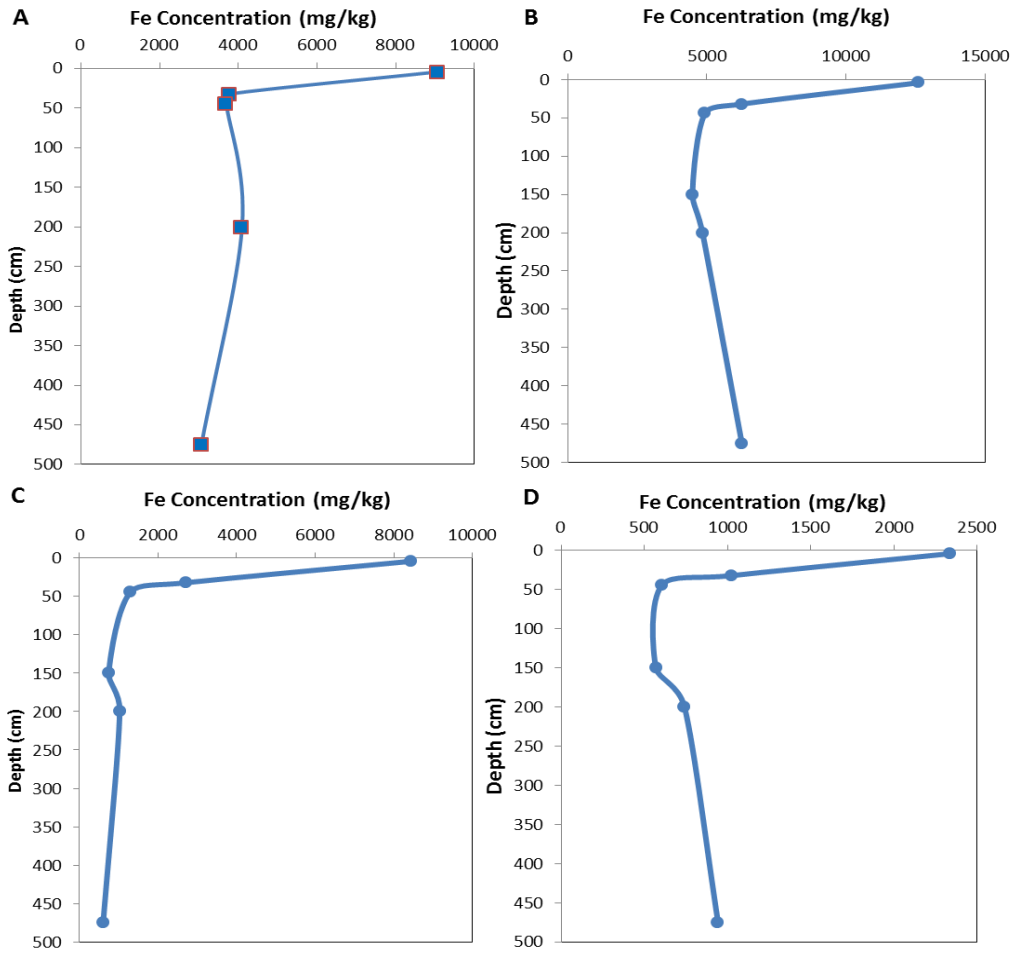

Figure 18: Al concentration depth profiles (A) Original samples from Earley, (B) Whole, untreated samples, (C) amorphous fractions and (D) solid samples after Ammonium Oxalate in the dark amorphous dissolution.

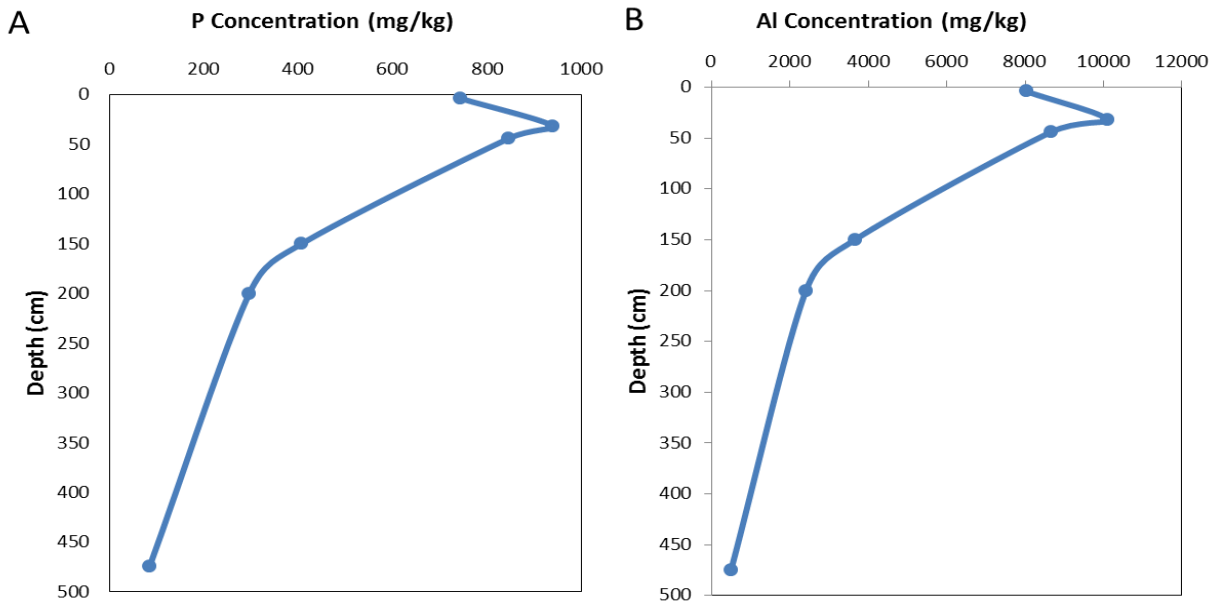

Figure 19: Depth Profiles of (A) Non-amorphous P and (B) Non-Amorphous Al. Profiles are congruent.

Examination of these depth profiles shows a strong congruence between non-amorphous Al and non-amorphous P (Figure 19). The amorphous depth profiles of Al and P do not show the same congruency, particularly in the 150-200 cm section of the core (Figure 20). We interpret this difference as an indicator that the correlation between Al and P occur in two modes: in the amorphous phase where P is sorbing and potentially co-precipitating with freshly precipitated

amorphous aluminum hydroxides phases.

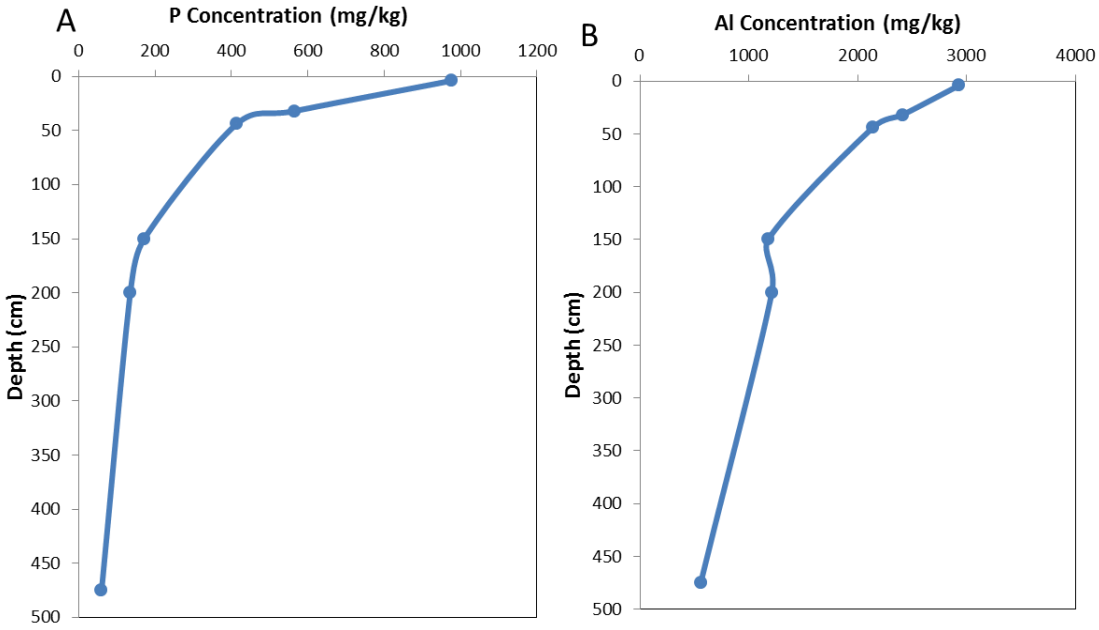

Figure 20: Depth Profiles of (A) Amorphous P and (B) Amorphous Al. Profiles are incongruent

This mechanism will not result in any strong congruency between the two concentrations but only a strong correlation as we have observed. The second mechanism is the one responsible for both the strong congruency and correlation that exist between Al and P in the non-amorphous phase and which is also the reason of the strong congruency and correlation observed in the total Al and P concentrations. In this case, we believe Al and P are indeed being inputted in the lake already bound together as a crystalline or at least non-amorphous phase. The inability of the XRD to detect such a phase could be related to its abundance and/or detection limit. Another possibility that we believe warrants further investigation in the future is the possibility that the Al and P correlation and depth congruency is related to the organic matter abundance and the paleo history of the lake. Figure 21 shows the depth profile of the organic matter in relation to Al and P concentrations in the original Earley's data.

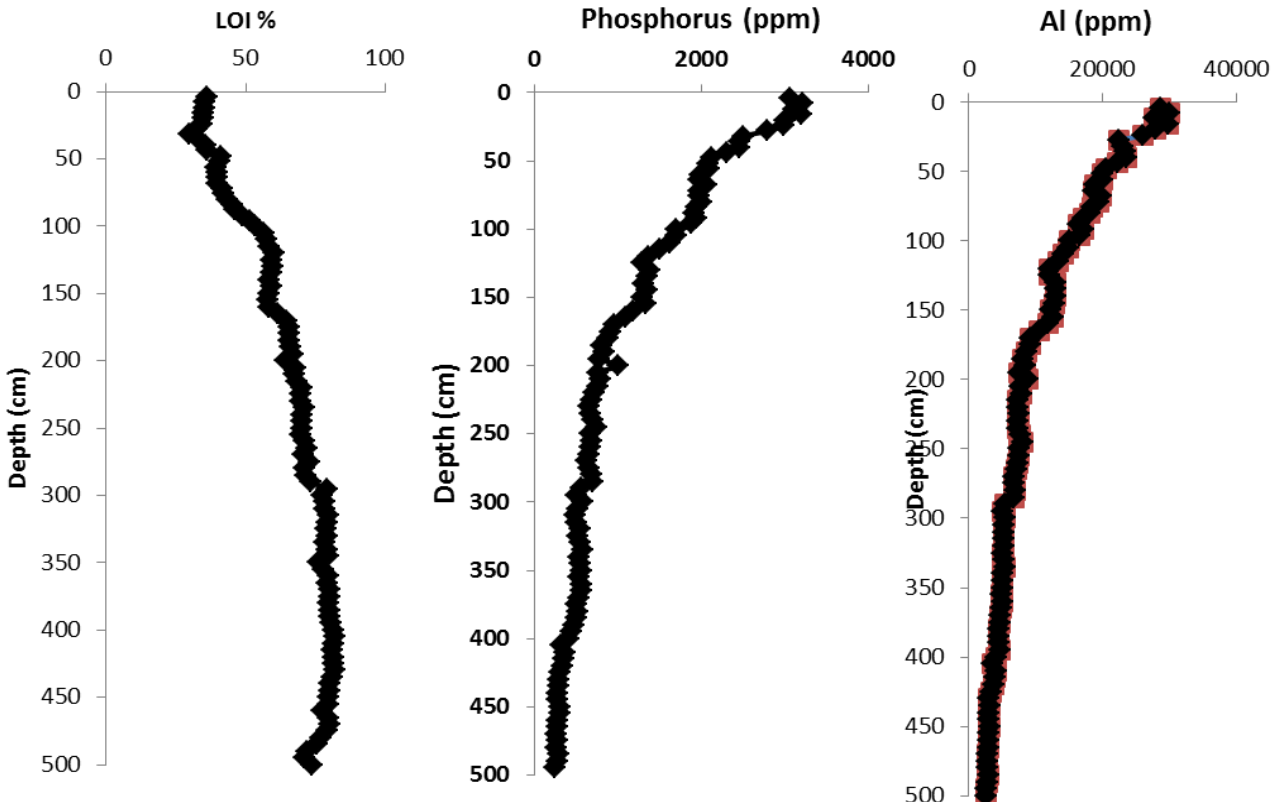

Figure 21: Depth Profiles of (A) Oraganic Matter measured by Percent Loss on Ignition, (B) Phosphorous concentrations and (C) Aluminum concentration. The Organic matter profile mirrors the P and Al, suggesting strong negative correlation. (Data from Waters/Earley)

In an attempt to further decouple the two "signals" of Al and P correlation in relation to the core depth and paleohistory, we calculated the ratio of concentrations from the liquid, amorphous phase collected after amorphous dissolution over the concentrations from the remaining solid, non-amorphous phase. A ratio greater than 1 represents an area of the core where the concentration of the amorphous phase is greater than the non-amorphous phase. We will refer to this ratio as the non-crystallinity ratio (NCR) for convenience with the understanding that it only represents the concentrations of these elements in these fractions and not a true measure of mineral crystallization. The NCR ratios are plotted against depth and are

shown in Figure 22.

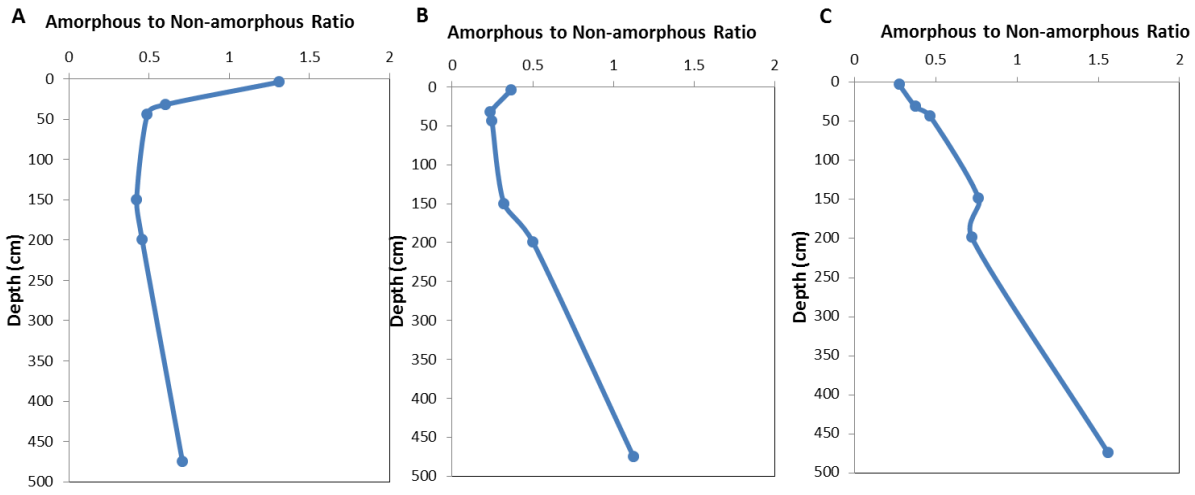

Figure 22: Amorphous to Non-amorphous ratio depth profiles for (A) P, (B) Al and (C) Fe. Ratios determined by dividing amorphous phase by non-amorphous phase. Ratios greater than 1 represent dominance of amorphous phase

A closer examination of these figures shows what appear to be 4 distinct zones of NCR behavior. From the bottom of the core until ~200 cm, the NCRs for P, Al and Fe decrease steadily, marking a concentration increase in the crystalline fraction. From ~ 200 cm to ~ 150 cm, the three elements behavior split. For P and Al, the NCR continues to decrease but at a slight slope change. For Fe, the NCR increase marking a concentration decrease in a crystalline fraction. From ~ 150 cm to ~50 cm, a noticeable reversal of trends is occurring. The NCR for P is increasing and the NCR for Al is just barely decreasing, marking what appears to be a significant zone of change in the chemical behavior of these elements. In that zone, the Fe NCR once again reverses trends and decreases. From ~ 50 cm depth to the top, the NCR for both P and Al see a rapid increase and hence a significant contributions of the P and Al concentrations in the amorphous fractions over those in the crystalline forms. The NCR of Fe continues to decrease as it proceeds upcore.

This behavior of the NCR across the 4 zones is reminiscent of the paleozones established earlier by Earley albeit not exactly the same. This analogous similarity suggests a potential impact of the shifting paleoenvironment on the physicochemical behavior of P, Al and Fe. It is possible that the organic matter through its high sorbing capacity and its effect on local pH (keeping it low) is influencing what elements remain in solution and hence precipitate when the pH is elevated to form the amorphous phases. In fact both Al and Fe amorphous phases are expected to precipitate at pHs higher than 5 (Bazilevskaya et al., 2011), often as co-precipitates with each other and with carbon forming assemblages with a complex behavior of chemistries depending on their relative solution concentrations. As these amorphous phases precipitate, they continue to sequester P rendering it unavailable to contribute to eutrophication.

SUMMARY AND CONCLUSION

In Long Pond, a strong correlation is seen between sedimentary Al and P. This correlation suggests that the abundant amounts of Al sequester most or all the P, limiting its availability to phytoplankton in the water and thus preventing eutrophication. After the samples were fractionated into amorphous and non-amorphous phases by amorphous dissolution, the correlation was maintained in both phases. Two modes of association between P and Al are suggested by this evidence. The first being a sorption and/or co-precipitation taking place in mainly the amorphous fraction. The other mode proposes detrital inputs of Al and P bound together before deposition. No evidence of crystalline mineral phases was discovered by XRD or SEM, possibly due to quantities and size of crystals being below detection limits.

Further investigation is needed on the role of the abundant organic matter present in the samples, and its effect on phosphorous and aluminum species in the lake sediments. Future study by a more thorough fractionation scheme that can measure the impacts of organic matter could provide answers.

The role of pH as it relates to the physicochemical properties of the Al and P relationship should not be overlooked, though it is beyond the scope of this study. A paleolimnological profile of changing pH conditions through history of Long Pond would elucidate possible conditions in which certain aluminophosphate mineral are likely to precipitate.

REFERENCES

Aspila, K. I., Agemian, H., & Chau, A. S. Y. (1976). A semi-automated method for the determination of inorganic, organic and total phosphate in sediments. *Analyst, 101*(1200), 187–197. http://doi.org/10.1039/AN9760100187

Bazilevskaya, E., Archibald, D. D., Aryanpour, M., Kubicki, J. D., & Martínez, C. E. (2011). Aluminum coprecipitates with Fe (hydr)oxides: Does isomorphous substitution of Al3+ for Fe3+ in goethite occur? *Geochimica et Cosmochimica Acta*, *75*(16), 4667–4683. http://doi.org/10.1016/j.gca.2011.05.041

Bennett, E. M., Carpenter, S. R., & Caraco, N. F. (2001). Human Impact on Erodable Phosphorus and Eutrophication: A Global Perspective Increasing accumulation of phosphorus in soil threatens rivers, lakes, and coastal oceans with eutrophication. *BioScience*, *51*(3), 227–234. http://doi.org/10.1641/0006-3568(2001)051[0227:HIOEPA]2.0.CO;2

Bohor, B. F., & Hughes, R. E. (1970). 19-1-49.pdf. Retrieved July 12, 2016, from http://www.clays.org/journal/archive/volume%2019/19-1-49.pdf

Buanuam, J., Miró, M., Hansen, E. H., & Shiowatana, J. (2006). On-line dynamic fractionation and automatic determination of inorganic phosphorus in environmental solid substrates exploiting sequential injection microcolumn extraction and flow injection analysis. *Analytica Chimica Acta*, *570*(2), 224–231. http://doi.org/10.1016/j.aca.2006.03.114

Busman, L., Lamb, J., Randall, G., Rehm, G., & Schmitt, M. (2002). The nature of phosphorus in soils. Regents of the University of Minnesota. Retrieved from http://www.extension.umn.edu/agriculture/nutrient-management/phosphorus/the-nature-of-phosphorus/

Colquhoun, D. J., Brooks, M. J., & Stone, P. A. (1995). Sea Level Fluctuation Emphais on Temporal Correlations. Retrieved June 28, 2016, from http://www.srarp.org/pdf_documents/Papers/MarkBrooks/Sea%20Level%20Fluctuation%20Emphais%20on%20Temporal%20Correlations_Colquhoun,%20Brook,%20and%20Stone%201995.pdf

Devau, N., Cadre, E. L., Hinsinger, P., Jaillard, B., & Gérard, F. (2009). Soil pH controls the environmental availability of phosphorus: Experimental and mechanistic modelling approaches. *Applied Geochemistry*, *24*(11), 2163–2174. http://doi.org/10.1016/j.apgeochem.2009.09.020

Dutrow, B. L., & Clark, C. M. (2008). X-ray Powder Diffraction (XRD). Retrieved July 13, 2016, from http://serc.carleton.edu/research_education/geochemsheets/techniques/XRD.html

Earley, S. M. (2015). Linking Biogeochemical Processes and Historic Primary Producer Communities: The Paleolimnology of Long Pond, Georgia, USA. Valdosta State University.

Frazier, W. J. (2016). Geologic Regions of Georgia: Overview. Retrieved July 15, 2016, from http://www.georgiaencyclopedia.org/articles/science-medicine/geologic-regions-georgia-overview

Frossard, E., Demaria, P., Sinaj, S., & Schärer, M. (2014). A flow-through reactor to assess potential phosphate release from agricultural soils. *Geoderma*, *219–220*, 125–135. http://doi.org/10.1016/j.geoderma.2013.12.015

GeorgiaInfo. (2016). physiomap.jpg (481×561). Retrieved July 19, 2016, from http://georgiainfo.galileo.usg.edu/images/uploads/gallery/physiomap.jpg

Hagerthey, S. E., Newman, S., Rutchey, K., Smith, E. P., & Godin, J. (2008). MULTIPLE REGIME SHIFTS IN A SUBTROPICAL PEATLAND: COMMUNITY-SPECIFIC THRESHOLDS TO EUTROPHICATION. *Ecological Monographs*, *78*(4), 547–565. http://doi.org/10.1890/07-0538.1

Huddlestun, P. F. (1997). Geologic Atlas of the Valdosta Area. Retrieved July 15, 2016, from https://epd.georgia.gov/sites/epd.georgia.gov/files/related_files/site_page/GA-10.pdf

Hyatt, J. A., & Gilbert, R. (2003). Subbottom acoustic and sedimentary records of past surface water?groundwater exchange through sinkhole lakes in south Georgia, U.S.A. *Environmental Geology*, *1*(1), 1–1. http://doi.org/10.1007/s00254-004-1010-7

Jalali, M., & Ranjbar, F. (2010). Aging effects on phosphorus transformation rate and fractionation in some calcareous soils. *Geoderma*, *155*(1–2), 101–106. http://doi.org/10.1016/j.geoderma.2009.11.030

Kawasaki, N., Ogata, F., & Tominaga, H. (2010). Selective adsorption behavior of phosphate onto aluminum hydroxide gel. *Journal of Hazardous Materials*, *181*(1–3), 574–579. http://doi.org/10.1016/j.jhazmat.2010.05.051

Kenney, W. F., Brenner, M., Curtis, J. H., Arnold, T. E., & Schelske, C. L. (2016). A Holocene Sediment Record of Phosphorus Accumulation in Shallow Lake Harris, Florida (USA) Offers New Perspectives on Recent Cultural Eutrophication. *PLOS ONE*, *11*(1), e0147331. http://doi.org/10.1371/journal.pone.0147331

Kenney, W. F., Waters, M. N., Schelske, C. L., & Brenner, M. (2002). Sediment records of phosphorus-driven shifts to phytoplanktondominance in shallow Florida lakes. *Journal of Paleolimnology*, *27*(3), 367–377. http://doi.org/10.1023/A:1016075012581

Kim, H.-S., Suhr, D.-S., Kim, G.-H., & Kum, D.-W. (1996). Analysis of X-ray diffraction patterns from mechanically alloyed Al-Ti powders. *Metals and Materials*, *2*(1), 15–21. http://doi.org/10.1007/BF03025942

Kim, L.-H., Choi, E., & Stenstrom, M. K. (2002). Sediment Characteristics, phosphorous types and phosphorous release rates between river and lake sediments. *Chemosphere*, *50*, 53–61.

McDowell, R. W., & Sharpley, A. N. (2003). Phosphorus solubility and release kinetics as a function of soil test P concentration. *Geoderma*, *112*(1–2), 143–154. http://doi.org/10.1016/S0016-7061(02)00301-4

Moore, R. C. R., Robert C. ,.Jr Reynolds Duane M. (1997). *X-Ray Diffraction and the Identification and Analysis of Clay Minerals* (2 SPI SUB edition). Oxford ; New York: Oxford Univ Pr.

Pecharsky, V., & Zavalij, P. (2008). *Fundamentals of Powder Diffraction and Structural Characterization of Materials, Second Edition* (2nd ed. 2009 edition). Berlin ; New York: Springer.

Petergans. (2008). *English: phosphoric acid speciation*. Retrieved from https://commons.wikimedia.org/wiki/File:Phosphoric3.png

Read, E. K., Ivancic, M., Hanson, P., Cade-Menun, B. J., & McMahon, K. D. (2014). Phosphorus speciation in a eutrophic lake by 31P NMR spectroscopy. *Water Research*, *62*, 229–240. http://doi.org/10.1016/j.watres.2014.06.005

Schindler, D. W. (1977). Evolution of Phosphorus Limitation in Lakes. *Science*, *195*(4275), 260–262. http://doi.org/10.1126/science.195.4275.260

Shariatmadari, H., Shirvani, M., & Jafari, A. (2006). Phosphorus release kinetics and availability in calcareous soils of selected arid and semiarid toposequences. *Geoderma*, *132*(3–4), 261–272. http://doi.org/10.1016/j.geoderma.2005.05.011

Sharpley, A., Smith, S., Jones, O., Berg, W., & Coleman, G. (1992). The Transport of Bioavailable Phosphorus in Agricultural Runoff. *Journal of Environmental Quality*, *21*(1), 30–35.

Sims, J. T., Simard, R. R., & Joern, B. C. (1998). Phosphorus loss in agricultural drainage: Historical perspective and current research. *Journal of Environmental Quality*, *27*(2), 277–293.

Spikatov, B. Y., Maryutina, T. A., & Muntau, H. (1999). Phosphorous Speciation in Water and Sediments. Retrieved July 13, 2016, from http://citeseerx.ist.psu.edu/viewdoc/download?doi=10.1.1.487.8968&rep=rep1&type=pdf

Temporetti, P., Snodgrass, K., & Pedrozo. (2013). Dynamics of phosphorus in sediments of a naturally acidic lake. *International Journal of Sediment Research*, *28*(1), 90–102. http://doi.org/10.1016/S1001-6279(13)60021-9

Tiessen, H. (Ed.). (1995). *Phosphorus in the Global Environment: Transfers, Cycles and Management* (1 edition). Chichester ; New York: Wiley.

Ulery, A. L., Drees, L. R., & America, S. S. S. of. (2008). *Methods of Soil Analysis: Mineralogical methods*. ASA-CSSA-SSSA.

Van Nieuwenhuyze, W., Roberts, S. J., Hodgson, D. A., Verleyen, E., Sterken, M., Sabbe, K., & Vyverman, W. (2014). Palaeolimnological reconstructions of mid-late Holocene climate change from South Georgia (Vol. 16, p. 14906). Presented at the EGU General Assembly

Conference Abstracts. Retrieved from http://adsabs.harvard.edu/abs/2014EGUGA..1614906V

Waters, M. N., Schelske, C. L., Kenney, W. F., & Chapman, A. D. (2005). The use of sedimentary algal pigments to infer historic algal communities in Lake Apopka, Florida. *Journal of Paleolimnology*, *33*(1), 53–71. http://doi.org/10.1007/s10933-004-1691-7

Welton, J. E. (2003). sem-atlas.pdf. Retrieved July 12, 2016, from http://www.doganaydal.com/nesneler/kutuphanekitaplar/sem-atlas.pdf

Xu, N., Li, Y., Zheng, L., Gao, Y., Yin, H., Zhao, J., … Chen, M. (2014). Synthesis and application of magnesium amorphous calcium carbonate for removal of high concentration of phosphate. *Chemical Engineering Journal*, *251*, 102–110. http://doi.org/10.1016/j.cej.2014.04.037

5 APPENDICES

Appendix A: Amorphous and Non-amorphous Phase Concentration Percentages and Mass Balance Recovery Calculations

Depth (cm)	Non-AOD P (µg/g)	AOD P (µg/g)	Total P (µg/g)	% Non-AOD	% AOD	Mass Balance recovery %
4	743	975	3855	19	25	75.61
32	939	564	2624	36	22	76.03
44	845	413	2419	35	17	72.40
150	407	171	1229	33	14	77.60
200	296	135	915	32	15	71.72
475	84	60	360	23	17	84.93

Depth (cm)	Non-AOD Al (µg/g)	AOD Al (µg/g)	Total Al (µg/g)	% Non-AOD	% AOD	Mass Balance recovery %
4	8026	2932	32846	24	9	51.49
32	10099	2410	26816	38	9	68.55
44	8658	2139	25067	35	9	64.56
150	3659	1178	13901	26	8	68.81
200	2410	1211	10147	24	12	68.40
475	496	558	4358	11	13	59.59

Depth (cm)	Non-AOD Fe (µg/g)	AOD Fe (µg/g)	Total Fe (µg/g)	% Non-AOD	% AOD	Mass Balance recovery %
4	8426	2336	12621	67	19	87.33
32	2705	1022	6245	43	16	60.73
44	1297	605	4934	26	12	68.42
150	743	569	4484	17	13	71.28
200	1024	741	4844	21	15	71.38
475	603	942	6259	10	15	78.30